J Solid State Electrochem (2001) 5: 375–381
DOI 10.1007/s100080000175

ORIGINAL PAPER

Shizhong Wang · Xinyu Lu · Meilin Liu

Electrocatalytic properties of an $Sr_{0.25}Bi_{0.5}FeO_{3-\delta}$/LSGM interface

Received: 28 April 2000 / Accepted: 30 August 2000 / Published online: 11 May 2001
© Springer-Verlag 2001

Abstract $Sr_{0.25}Bi_{0.5}FeO_{3-\delta}$ (SBF) has been studied as a cathode material for low- and intermediate-temperature (600–850 °C) solid oxide fuel cells (SOFCs) based on the $La_{0.9}Sr_{0.1}Ga_{0.9}Mg_{0.1}O_3$ (LSGM) electrolyte. The observed cathodic current density passing through an SBF/LSGM interface at 840 °C in pure oxygen is about 1 $A{\cdot}cm^{-2}$ at an overpotential of 40 mV, much higher than that for an $La_xSr_{1-x}MnO_3$ electrode under similar conditions reported in the literature. Analysis indicates that the electrode kinetics is controlled primarily by mass transfer at high temperatures and by charge transfer at low temperatures. The inductive loops of the impedance spectra further suggest that the adsorption of intermediate species is involved in the interfacial reaction.

Keywords Oxygen reduction · Cathode · Mechanism · Mixed conductor · SOFCs

Introduction

Solid oxide fuel cells (SOFCs) have emerged as a leading technology to provide advanced power sources in an environmentally clean and efficient manner. Low operating temperature (600–850 °C) is important to significantly reduce the material and maintenance cost, which is necessary for the commercialization of SOFC technology. However, the performance of SOFCs decreases dramatically as the operating temperature is reduced because of high activation energy of interfacial processes. Thus, it is essential to develop new electrode materials with high catalytic activity at low and intermediate temperatures [1, 2, 3, 4].

It is well known that a mixed ionic-electronic conductor (MIEC) has great potential to enhance electrode kinetics of solid-state cells because it may extend the active reaction region from the three-phase boundary (TPB) to the surface of the porous MIEC [4, 5, 6, 7]. Several MIECs (such as $La_{0.6}Sr_{0.4}CoO_{3-\delta}$ [8] and $La_{1-x}Sr_xFe_yCo_{1-y}O_{3-\delta}$ [9]) have been reported to be promising cathode materials. To effectively use the surface of an MIEC electrode, the MIEC must have fast ionic and electronic transport in addition to adequate stability, high catalytic activity, and thermal and chemical compatibility with the electrolyte materials [10]. Recent studies showed that $Sr_{0.25}Bi_{0.5}FeO_{3-\delta}$ (SBF) displays high oxygen permeability at low temperatures and exhibits remarkable stability even in a reducing atmosphere, implying that the SBF is a promising electrode material for SOFCs [11].

The overall reaction for electrochemical reduction of oxygen in a cell based on a solid oxide electrolyte containing oxygen vacancies (such as LSGM) can be expressed as [12, 13]

$$1/2O_{2(gas)} + 2e^- + V_{O,ele}^{\cdot\cdot} \rightarrow O_{O,ele}^{X} \quad (1)$$

where $V_{O,ele}^{\cdot\cdot}$ and $O_{O,ele}^{X}$ stand for an oxygen vacancy and an oxygen ion at a regular oxygen site in the electrolyte, respectively. In general, two parallel pathways should be considered for oxygen reduction when a porous MIEC is used as electrode, the TPB and the MIEC/gas interface [5]. In many cases, however, it is the TPB that dominates the electrode kinetics.

Phenomenologically, the relationship between the current passing through an electrode/electrolyte interface, i, and the overpotential across the interface, η, can be described by the Butler-Volmer equation,

$$i = i_0\left[\exp\left(\frac{\alpha_a F\eta}{RT}\right) - \exp\left(-\frac{\alpha_c F\eta}{RT}\right)\right] \quad (2)$$

S. Wang · X. Lu · M. Liu (✉)
School of Material Science and Engineering,
Georgia Institute of Technology,
Atlanta, GA 30332, USA
E-mail: meilin.liu@mse.gatech.edu
Tel.: +1-404-8946114
Fax: +1-404-8949140

where i_0 is the exchange current density, F is the Faraday's constant, R is the universal gas constant, T is the absolute temperature, and α_a and α_c are the anodic and cathodic charge transfer coefficients. The α_a and α_c are related to the number of electrons involved in the overall reaction, n, and the number of times the rate-determining step (rds) occurs for one act of the overall reaction, *v*, as follows

$$\alpha_a + \alpha_c = n/v \tag{3}$$

When the overpotential is sufficiently small, i.e., [arrowvertex]η[arrowvertex] < < (RT/F), Eq. 2 simplifies to,

$$i \approx i_0(\alpha_a + \alpha_c)\frac{F\eta}{RT} \tag{4}$$

Under this condition, the interfacial resistance can be approximated by

$$R_p = \left(\frac{\partial\eta}{\partial i}\right) = \left(\frac{RT}{F}\right)\left(\frac{1}{\alpha_\alpha + \alpha_c}\right)\left(\frac{1}{i_0}\right) \tag{5}$$

which can be readily determined from an impedance spectrum [14]. The exchange current density can then be calculated from R_p as

$$i_o = \frac{RT}{F}\left(\frac{1}{\alpha_\alpha + \alpha_c}\right)\left(\frac{1}{R_p}\right) \tag{6}$$

When the overpotential is sufficiently high ([arrowvertex]η[arrowvertex] > > RT/F), Eq. 2 simplifies to

$$i \approx -i_0 \exp\left(-\alpha_c \tfrac{F\eta}{RT}\right); \quad \eta < 0 \tag{7a}$$

or

$$i \approx i_0 \exp\left(\alpha_a \tfrac{F\eta}{RT}\right); \quad \eta > 0 \tag{7b}$$

Thus, the cathodic and anodic charge transfer coefficients can be determined from

$$\alpha_c = \frac{RT}{F}\frac{1}{(-\eta)}\ln\left|\frac{i}{i_0}\right| \tag{8a}$$

and

$$\alpha_a = \frac{RT}{F}\frac{1}{\eta}\ln\left|\frac{i}{i_0}\right| \tag{8b}$$

In this paper, we report the characteristics of oxygen reduction at an SBF/LSGM interface as studied using DC polarization and impedance spectroscopy. In particular, the interfacial polarization resistance, R_p, exchange current density, i_0, and the charge transfer coefficients, α_a and α_c, are determined to elucidate the reaction mechanisms and evaluate the suitability of using SBF as a cathode for SOFCs based on LSGM electrolytes.

Materials and methods

A conventional ceramic process was used to prepare the LSGM electrolyte [15] and the SBF electrode [11]. La_2O_3, $SrCO_3$, Ga_2O_3, and MgO were used as precursors for the preparation of the $La_{0.9}Sr_{0.1}Ga_{0.9}Mg_{0.1}O_3$ (LSGM) electrolyte [15]. Powders with stoichiometric composition were ball-milled in ethanol for 24 h and calcined at 1100 °C for 5 h to form the perovskite phase. X-ray powder diffraction (Philips, PW 1800) was used to characterize the phase composition of the calcined products. Powders with the perovskite phase were crushed using an agate motor and pestle and then ball-milled in ethanol for 24 h. The resulting fine powders were pressed into pellets (with 20 mm in diameter and 1 mm in thickness) under 400 atm for 1 minute and sintered at 1500 °C for 6 h. The sintered density of the LSGM pellets is greater than 95% of the theoretical value. Precursors for SBF were $SrCO_3$ (98 + %), Bi_2O_3 (99.9%), and Fe_2O_3 (99 + %), all from Aldrich Chemical Company. Stoichiometric amounts of precursors were ball-milled in ethanol for 24 h, and then calcined in air at 800 °C for 10 h to form a perovskite phase of SBF. The phase compositions of the calcined products were confirmed using X-ray diffraction.

A three-electrode configuration [7] was used for electrochemical measurements. The SBF powder was mixed with appropriate amounts of organic binder and solvent to form an SBF paste, which was screen-printed on one side of the electrolyte as the working electrode. The superficial area and the thickness of the working electrode after firing were about 0.3 cm^2 and 10∼30 μm, respectively. Pt counter and reference electrode were prepared by screen-printing of Pt paste (Engelhard) on the other side of the electrolyte followed by firing at 950 °C for 2 h. The areas of the counter and the reference electrodes were about 0.8 and 0.1 cm^2, respectively. Platinum grids were attached and pressed with springs on the working and counter electrodes as the current collector. Three Pt wires were connected to the working, counter, and reference electrodes, respectively, and led to a potentiostat/galvanostat. The entire cell was immersed in a uniform atmosphere having different partial pressures of oxygen during electrochemical measurements using an EG & G 273A potentiostat/galvanostat and a 5201 lock-in amplifier. The flow rate of the inlet gas was about 100 $ml \cdot min^{-1}$. The frequency range of impedance measurements was from 0.01 Hz to 100 kHz, and the amplitude of the input sine-wave signal was 5 mV. The microstructures of the investigated samples were examined using a scanning electron microscope (SEM, Hitachi S-800).

Results and discussion

Microstructure of electrode and electrode/electrolyte interface

Shown in Fig. 1 are several SEM micrographs of the surface view of an SBF electrode and the cross-sectional view of an SBF/LSGM interface. The SBF electrode has a porous structure with a porosity of about 30–40% and the average size of the SBF grains is about 1 μm. The adhesion of the SBF electrode layer to the LSGM electrolyte appears to be good and the thickness of the electrode layer is about 25 μm.

Impedance spectroscopy and *dc* polarization near equilibrium

Shown in Fig. 2 are the impedance spectra of an SBF/LSGM interface (without DC bias) measured at

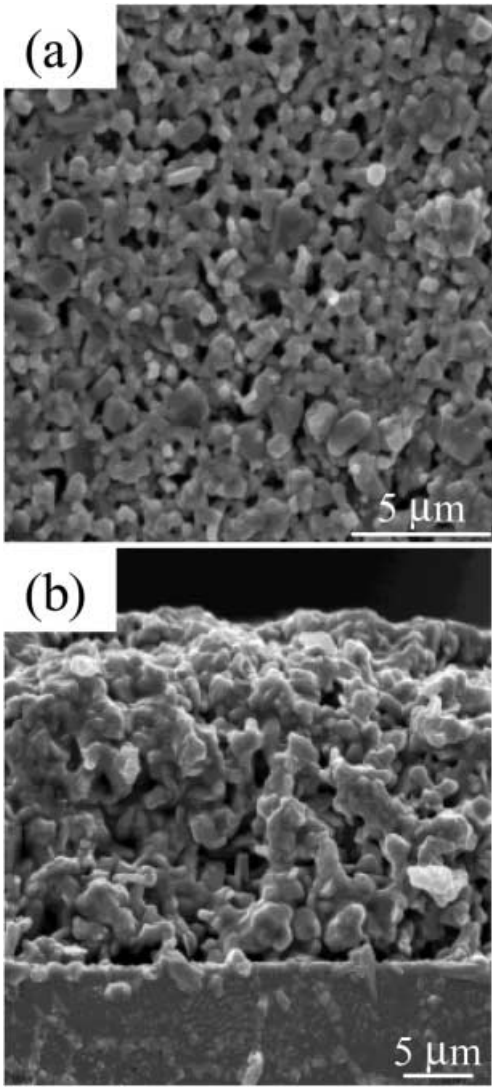

Fig. 1 Typical SEM micrographs of **a** an SBF surface and **b** an SBF/LSGM interface, fired at 950 °C for 2 h

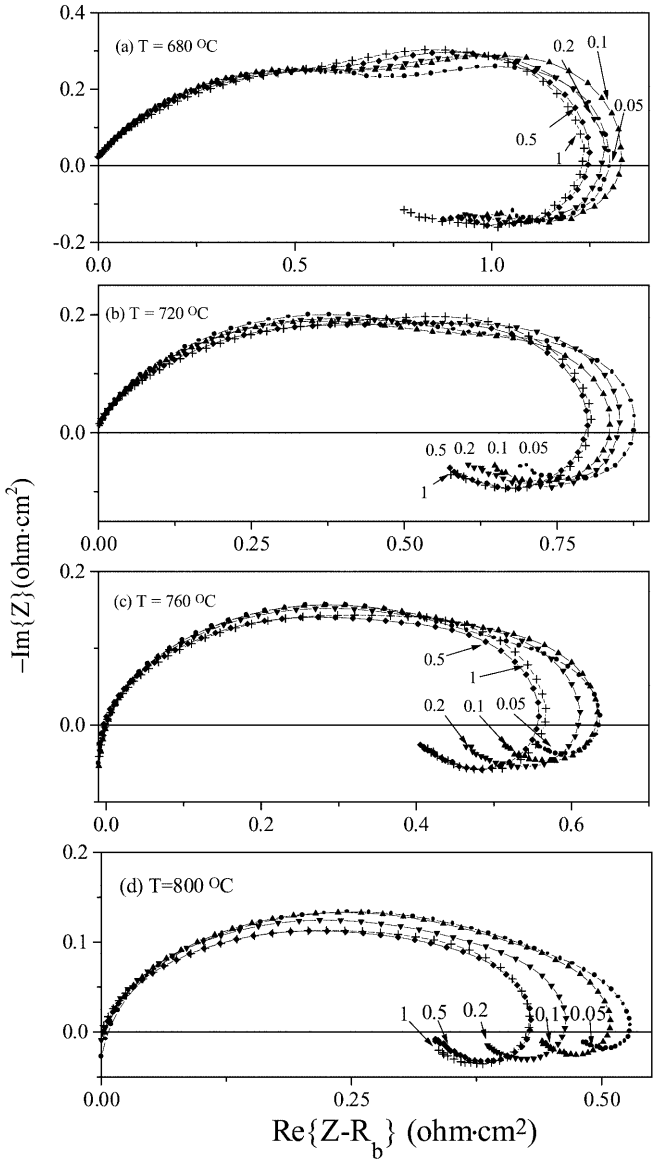

Fig. 2a–d Impedance spectra of an SBF/LSGM interface measured at different temperatures and oxygen partial pressures under equilibrium conditions (without DC bias). The number adjacent to each spectrum represents the partial pressure of oxygen in atm

different temperatures (680, 720, 760, and 800 °C) in atmospheres having different partial pressures of oxygen (1.0, 0.5, 0.2, 0.1, and 0.05 atm). All cell impedances (Z) were normalized by the superficial electrode area so that they have a unit of $\Omega \cdot cm^2$. The bulk resistance of each cell (R_b) was subtracted from the total cell impedance to reveal the interfacial impedance ($Z–R_b$) under the testing conditions.

An obvious inductive loop was observed in most of the impedance spectra. The size of the inductive loop, as determined from the spectra shown in Fig. 2, is presented in Fig. 3 as a function of the partial pressure of oxygen. Since the sizes of the inductive loops decreased with temperature but increased with the partial pressure of oxygen, they must be related to the intrinsic properties of the SBF/LSGM interface, not induced by on-line induction (leading wires) or other artificial effects. Further, the size of the inductive loop decreased rapidly with the increase in the value of the anodic overpotential (see Fig. 4), but was relatively insensitive to the value of the cathodic overpotential up to –30 mV. The impedance analysis near equilibrium indicates that the kinetics of oxygen reduction at an SBF/LSGM interface is controlled primarily by a charge-transfer process under low-polarization.

Inductive loops have been observed in many electrochemical systems involving liquid electrolytes, such as the dissolution of iron [16, 17], oxygen evolution on composite electrodes in an Na_2SO_4 solution [18], and oxygen reduction at a platinum electrode in an alkaline electrolyte [19]. The theoretical analyses of the inductive behavior [22] attributed the inductive loop to the involvement of active adsorbed intermediate species in the reaction. Recently, inductive loops were also observed in

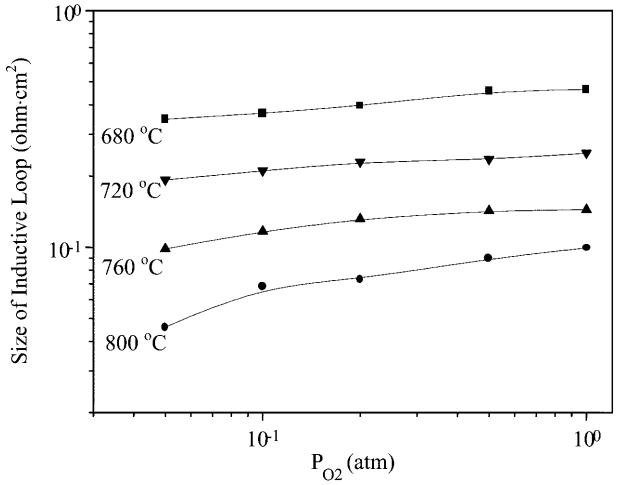

Fig. 3 The sizes of the inductive loops as a function of temperature and the partial pressure of oxygen

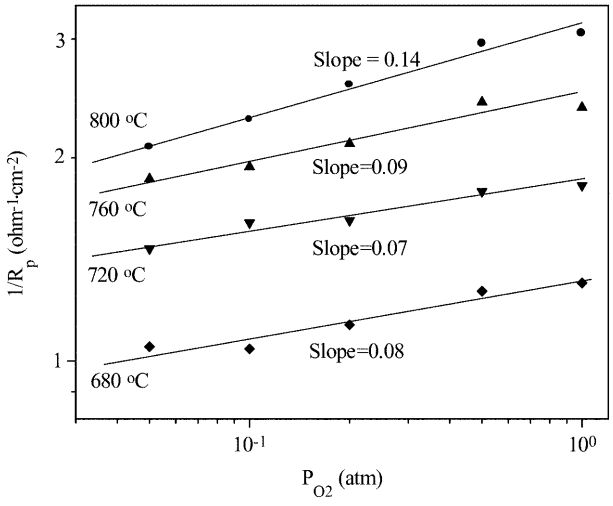

Fig. 5 The dependence of the interfacial resistance on the partial pressure of oxygen at different temperatures (calculated from the data presented in Fig. 2)

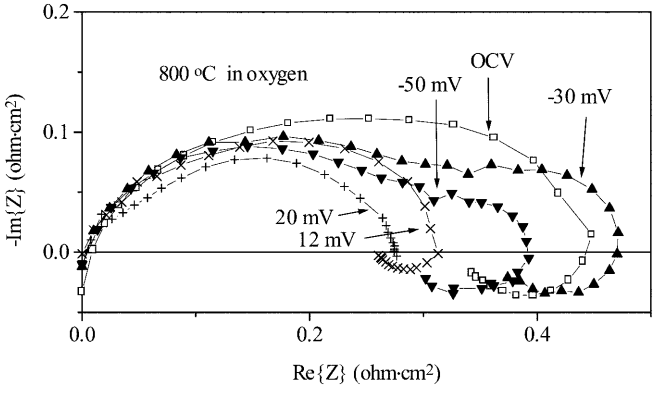

Fig. 4 Effect of the value of the *dc* polarization on the size of the inductive loops observed in impedance spectra measured at 800 °C in pure oxygen

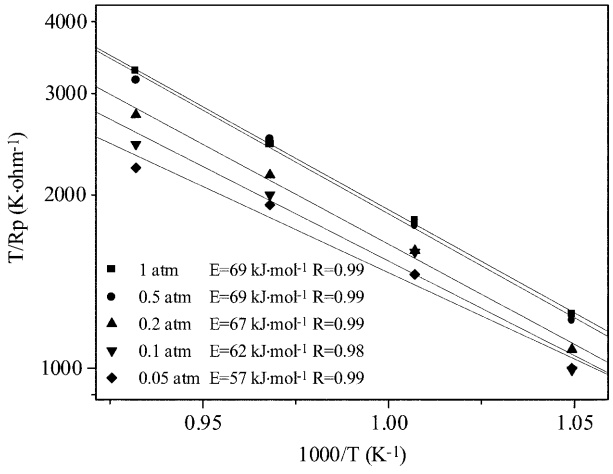

Fig. 6 The dependence of the interfacial resistance on temperature and the partial pressure of oxygen (calculated from the data presented in Fig. 2), where E represents the activation energy and R represents the correlation coefficient

solid-state electrochemical systems, such as the electrochemical reduction of oxygen at an LSM/YSZ interface [20, 21]. However, the inductive behavior observed in solid-state systems has not been well understood. It is believed that several kinds of adsorbed intermediate species might be involved in the overall oxygen reduction over Pt or LSM electrodes, such as O^-_{ads}, O^-_{adsTPB}, O^{-2}_{ads} [12, 13]. The reduction of oxygen over a mixed conductor is even more complex, which could involve other kinds of adsorbed intermediate species, such as O^{-2}_{ads}. The detailed mechanism is yet to be identified.

The interfacial polarization resistances were obtained from the impedance of the inductive loop at low frequency limit ($\omega \rightarrow 0$), which were in good agreement with the resistances measured using *dc* polarization. Shown in Fig. 5 are the reciprocal of the interfacial resistances determined from Fig. 2. The polarization resistance (R_p) of the SBF/LSGM interface decreased slightly with the partial pressure of oxygen. The slope of $1/R_p$ vs. P_{O2} varied from 0.14 to 0.08 as the temperature was changed from 800 to 680 °C.

Shown in Fig. 6 is the dependence of T/R_p or i_0 on temperature for an SBF/LSGM interface. The calculated activation energy for exchange current density i_0 varied from 57 to 69 kJ·mol^{-1} as the partial pressure of oxygen varied from 0.05 to 1 atm. The observed activation energies for the SBF electrode are much lower than those for Pt and LSM electrodes [12, 24].

The dependence of activation energy on the partial pressure of oxygen might be due to the involvement of adsorption heat in the apparent activation energy of exchange current density [24]. Under the assumption that the reaction at the SBF/LSGM interface is controlled by a charge-transfer process, the exchange current density can also be expressed as [12, 24],

$$i_0 = 2FK_r[\theta_O(1-\theta_O)]^{1/2} \quad (9)$$

where K_r is the reaction constant and θ_0 is the coverage of oxygen atoms at the SBF/LSGM interface, and is given by

$$\theta_O = \frac{(bP_{O2})^{1/2}}{1 + (bP_{O2})^{1/2}} \tag{10}$$

where $b = k_f/k_b$, which is a constant for the adsorption/desorption of oxygen. Combination of Eq. 9 and Eq. 10 yields

$$i_0 = \frac{2FK_r(bP_{O2})^{1/4}}{1 + (bP_{O2})^{1/2}} \tag{11}$$

implying that the dependence of exchange current density on the partial pressure of oxygen can vary from 1/4 to –1/4, depending on the value of bP_{O2}.

Impedance spectroscopy and *dc* polarization far away from equilibrium

High overpotential polarization was carried out at 840 °C and 720 °C in an atmosphere having an oxygen partial pressure of 0.2, 0.5, and 1.0 atm, respectively. The bulk resistances of the cell were measured using impedance spectroscopy at each point in order to correct the IR drop in *dc* polarization measurements. All *dc* measurements were acquired in a steady state; it takes about 20 minutes for the system to reach equilibrium under each testing condition. Impedance spectra were recorded under the same conditions for the *dc* polarization measurement.

Shown in Fig. 7 are the current-overpotential curves for an SBF/LSGM interface, indicating that SBF is a promising electrode material with a high catalytic activity for oxygen reduction. In pure oxygen, the observed cathodic current density reached 1 $A{\cdot}cm^{-2}$ at an overpotential of 40 mV at 840 °C and 0.5 $A{\cdot}cm^{-2}$ at an overpotential of 100 mV at 720 °C. These current density values are much higher than those observed on an $La_xSr_{1-x}MnO_3$ electrode under similar conditions (about 0.5 $A{\cdot}cm^{-2}$ at an overpotential of 40 mV at 950 °C in oxygen) [7, 13].

The anodic polarization curves shown in Fig. 7 display a clear Tafel region. At 840 °C, the anodic charge transfer coefficients were about 0.8 without observable dependence on the partial pressure of oxygen. At 720 °C (Table 1), however, the anodic charge transfer coefficients increased from 0.7 to about 1 as the partial pressure of oxygen was increased from 0.2 to 1 atm. In contrast, the cathodic polarization curves observed at 840 °C [Fig. 7 (a)] do not display a Tafel region, due probably to the small range of overpotentials applied in the experiment. However, a well-defined Tafel region is observed in the cathodic polarization curves at 720 °C [Fig. 7 (b)]; the charge transfer coefficients vary from about 1 to 1.5, depending strongly on the partial pressure of oxygen (Table 1).

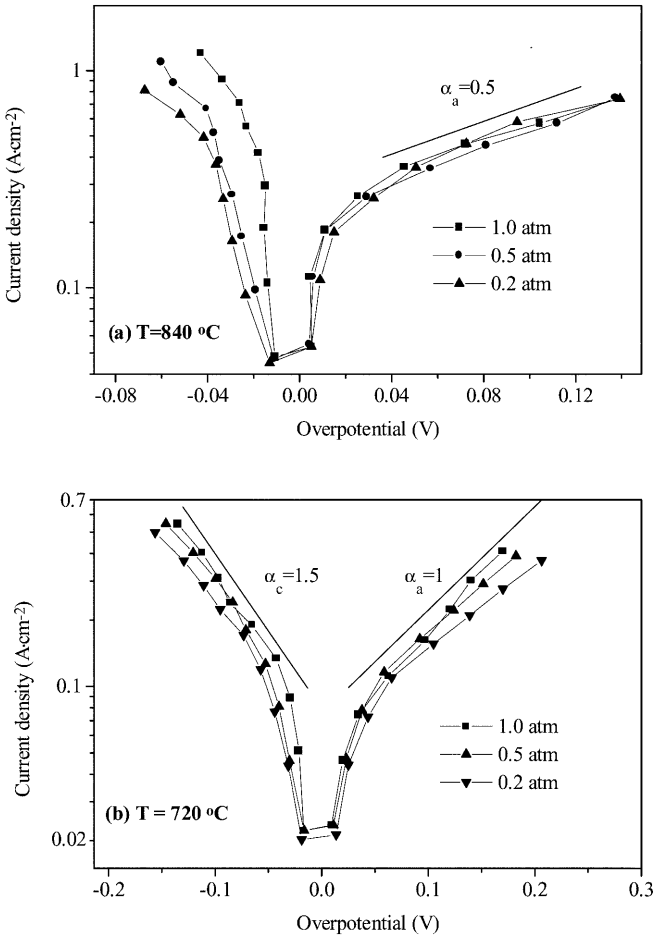

Fig. 7 Polarization curves for an SBF/LSGM interface as measured **a** at 840 °C and **b** at 720 °C

Table 1 Charge-transfer coefficients estimated from the data presented in Fig. 7

T (°C)	720			840		
P_{O2} (atm)	1	0.5	0.2	1	0.5	0.2
α_a	1.0	0.8	0.7	0.7	0.8	0.7
α_c	1.4	1.2	1.1			

Shown in Fig. 8 are some typical impedance spectra of an SBF/LSGM interface measured in pure oxygen at 720 °C under the influence of a *dc* polarization. Two arcs were observed in each impedance spectrum, the size of the low-frequency arc decreased rapidly with the value of *dc* polarization, implying that this arc is closely related to the charge-transfer process. The size of the arc at high frequencies was relatively insensitive to the value of the applied *dc* polarization, suggesting that the arc at high frequencies corresponds probably to bulk transport. Since the size of the low-frequency arc was much greater than that of the high-frequency arc under low polarization, the rate of the overall interfacial process is controlled mainly by charge transfer process under these

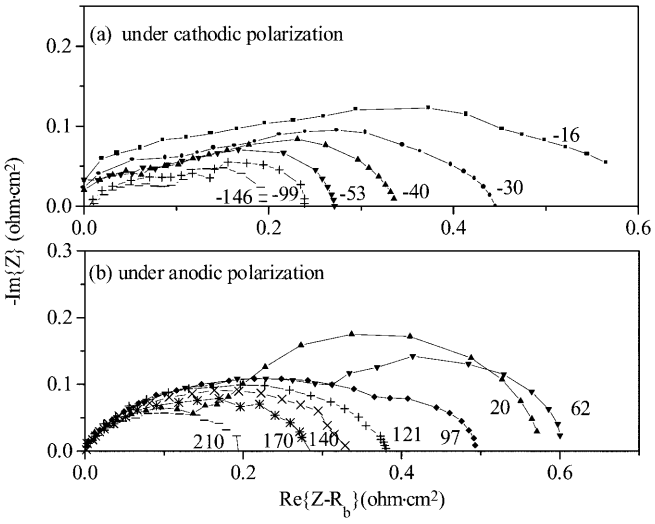

Fig. 8a, b Impedance spectra of an SBF/LSGM interface (measured at 720 °C in pure oxygen) under the influence of a *dc* polarization. The number adjacent to each spectrum represents the value of the applied *dc* bias in mV

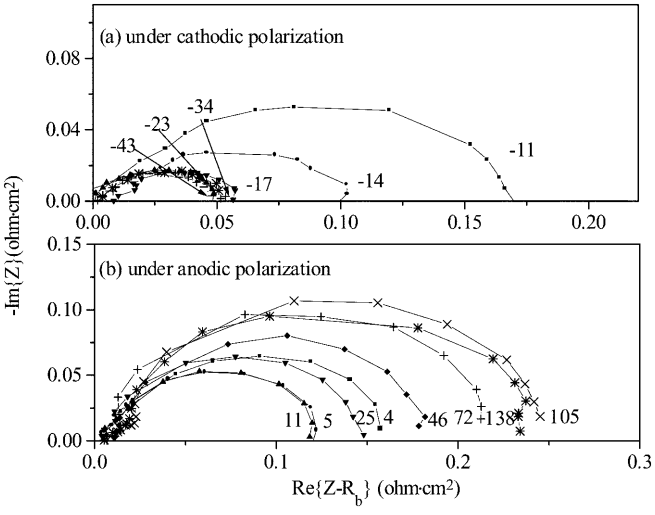

Fig. 9a, b Impedance spectra of an SBF/LSGM interface (measured at 840 °C in pure oxygen) under the influence of a *dc* polarization. The number adjacent to each spectrum represents the value of the applied *dc* bias in mV

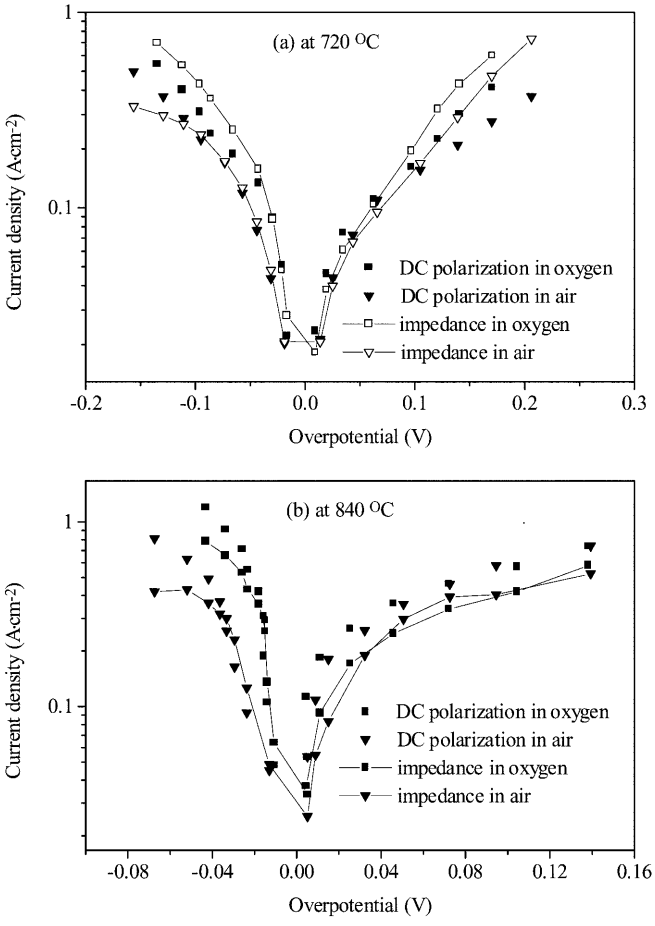

Fig. 10 Polarization curves determined from *dc* polarization and from impedance spectroscopy in pure oxygen and air: **a** at 840 °C and **b** at 720 °C

conditions. The impedance spectra measured in air at 720 °C were similar to those measured in pure oxygen. However, the impedance in air increased slightly with the value of *dc* overpotential when the overpotential was higher than 0.3 V or lower than –0.1 V, which was due possibly to the effect of mass transfer.

The impedance spectra under cathodic and anodic polarization at 840 °C in pure oxygen are shown in Fig. 9. There are also two arcs in each spectrum. The impedance of the low-frequency arc was much greater than that of the high-frequency arc. The size of the low-frequency arc decreased with the value of the applied overpotential under low polarization, and remained stable with the further increase of the overpotential. It seemed that the *rds* for oxygen reduction changed from charge transfer to mass transfer with the increase of the value of the *dc* polarization. The impedance spectra measured at 840 °C in air were similar to those measured in oxygen, except that the effect of mass transfer was more obvious in the former case. These results suggest that the rate of the oxygen reduction at an SBF/LSGM interface is controlled by mass transfer at high temperatures under high overpotentials. Therefore, the Tafel region observed in Fig. 7 (a) was a pseudo-Tafel curve due to the diffusion of oxygen species. This is a common phenomenon in oxygen reduction on MIECs, which has been analyzed in detail by Nisancioglu et al. [23].

Compared with the impedance spectra under cathodic polarization [Fig. 8 (a) and Fig. 9 (a)], it can be seen that the anodic reaction [Fig. 8 (b) and Fig. 9(b)] is more strongly influenced by the mass transfer processes. This can be explained as follows. The polarity of polarization may directly influence the concentration of oxygen vacancies; Oxygen vacancies are generated under cathodic polarization while consumed under anodic polarization. It is most likely that the oxygen vacancies

contribute greatly to the diffusion of intermediate oxygen species, which can extend the active sites from the TPB to the surface of electrode. This agrees with the results of *dc* polarization shown in Fig. 7, i.e., under high overpotentials, the cathodic current is much higher than the anodic current under the same value of the overpotential.

Shown in Fig. 10 are the polarization curves constructed from impedance data; also shown in this figure are the polarization curves obtained from *dc* polarization under the same conditions. At 720 °C, the cell currents calculated from impedance data were slightly higher than those determined from *dc* polarization except the cathodic polarization curve in an atmosphere with the partial pressure of oxygen of 0.2 atm; while at 840 °C, the cell currents calculated from impedance data were slightly lower than those determined from *dc* polarization. The small differences between the *ac* and *dc* polarization measurements were due to the relaxation under high overpotentials. It was noticed that the current passing through an SBF/LSGM interface increased with time slightly at low temperatures under a steady-state polarization while decreased with time at high temperatures. This could be related to the change of reaction pathways or the change of intrinsic properties of the SBF/LSGM interface or the SBF electrode with temperatures. Similar phenomena were also observed in the investigation of LSM electrodes [13].

Conclusions

$Sr_{0.25}Bi_{0.5}FeO_{3-\delta}$ (SBF) exhibits high catalytic activity for oxygen reduction at low and intermediate temperatures; the observed cathodic current density passing through an SBF/LSGM interface at 840 °C in pure oxygen reaches 1 $A{\cdot}cm^{-2}$ at an overpotential of 40 mV. The overall rate of the reaction is controlled primarily by mass transfer at high temperatures and by charge transfer at low temperatures. Significant inductive loops are observed in the impedance spectra, indicating that adsorbed intermediate species are involved in the reaction. SBF is a very attractive candidate for cathode material in low and intermediate-temperature SOFCs or other solid-state ionic devices based on LSGM electrolytes.

Acknowledgements This work was supported by National Science Foundation under Grant No. CTS-9705541 and CTS-9819850.

References

1. Feng M, Goodenough JB, Huang K, Milliken C (1996) J Power Sources 63:47
2. Ishihara T, Honda M, Shibayama T, Minami H, Nishiguchi H, Takita Y (1998) J Electrochem Soc 145:3177
3. Ishihara T, Kudo T, Matsuda H, Takita Y (1995) J Electrochem Soc 142:1519
4. Uchida H, Yoshida M, Watanabe M, Watanabe M (1999) J Electrochem Soc 146:1
5. Liu M (1998) J Electrochem Soc 145:142
6. Lee HY, Cho WS, Oh SM (1995) J Electrochem Soc 142: 2660
7. Wang S, Jiang Y, Zhang Y, Yan J, Li W (1998) J Electrochem Soc 145:1932
8. Kawada T, Masuda K, Suzuki J, Kaimai A, Kawamura K, Nigara Y, Mizusaki J, Yugami H, Arashi H, Sakai N, Yokokawa H (1998) Solid State Ionics 121:271
9. Sirman JD, Kilner JA (1996) J Electrochem Soc 143:L229
10. Minh NQ, Takahashi T (1995) Science and Technology of Ceramic Fuel Cells. Elsevier Science BV, Amsterdam
11. Lu X, Liu M (1999) Electrochemical and Solid-State Letters 2:452
12. Wang D, Nowick AS (1970) J Electrochem Soc 126:1115
13. Heuveln Van FH, Bouwmeester HJM (1997) J Electrochem Soc 144:134
14. Hu H, Liu M (1997) J Electrochem Soc 144:3561
15. Chen F, Liu M (1998) J Solid State Electrochem 3:7
16. Keddam M, Mattos OR, Takenouti H (1981) J Electrochem Soc 128:257
17. Keddam M, Mattos OR, Takenouti H (1981) J Electrochem Soc 128:266
18. Darowicki K, Orlikowski J (1999) J Electrochem Soc 146:663
19. Zhou DB, Poorten HV (1998) J Electrochem Soc 145:936
20. Juhl M, Primdahl S, Mason C, Mogensen M (1996) J Power Sources 61:173
21. Gharbage B, Pagnier T, Hammou A (1994) J Electrochem Soc 141:2118
22. Bai L, Conway BE (1991) J Electrochem Soc 138:2897
23. Svensson AM, Sunde S, Nisancioglu K (1998) J Electrochem Soc 145:1390
24. Jiang Y, Wang S, Zhang Y, Yan J, Li W (1998) Solid State Ionics 110:111